STEM CELLS TRANSLATIONAL MEDICINE®

ENABLING TECHNOLOGIES FOR CELL-BASED CLINICAL TRANSLATION

Biodistribution and Clearance of Human Mesenchymal Stem Cells by Quantitative Three-Dimensional Cryo-Imaging After Intravenous Infusion in a Rat Lung Injury Model

ERIC G. SCHMUCK,[a] JILL M. KOCH,[b] JOHN M. CENTANNI,[a] TIMOTHY A. HACKER,[b] RUDOLF K. BRAUN,[c] MARLOWE ELDRIDGE,[c] DEREK J. HEI,[d] PEIMAN HEMATTI,[e,f] AMISH N. RAVAL[a,g]

Key Words. Biodistribution • Mesenchymal stem cell • Cell tracking • Quantum dots • Lung injury • Cryo-imaging

[a]Department of Medicine, Division of Cardiovascular Medicine, [b]Cardiovascular Research Center, and [e]Department of Medicine, Division of Hematology/Oncology, University of Wisconsin School of Medicine and Public Health, Madison, Wisconsin, USA; [c]Department of Pediatrics and [g]Department of Biomedical Engineering, University of Wisconsin, Madison, Wisconsin, USA; [d]Waisman Biomanufacturing, Madison, Wisconsin, USA; [f]University of Wisconsin Carbone Cancer Center, Madison, Wisconsin, USA

Correspondence: Eric G. Schmuck, Ph.D., Department of Medicine, Division of Cardiovascular Medicine, 8526 Wisconsin Institute for Medical Research Tower 2, 1111 Highland Avenue, Madison, Wisconsin 53792, USA. Telephone: 608-263-9449; E-Mail: egs@medicine.wisc.edu

Received December 1, 2015; accepted for publication May 13, 2016; published Online First on July 26, 2016.

1066-5099/2016/$20.00/0

http://dx.doi.org/10.5966/sctm.2015-0379

ABSTRACT

Cell tracking is a critical component of the safety and efficacy evaluation of therapeutic cell products. To date, cell-tracking modalities have been hampered by poor resolution, low sensitivity, and inability to track cells beyond the shortterm. Three-dimensional (3D) cryo-imaging coregisters fluorescent and bright-field microcopy images and allows for single-cell quantification within a 3D organ volume. We hypothesized that 3D cryo-imaging could be used to measure cell biodistribution and clearance after intravenous infusion in a rat lung injury model compared with normal rats. A bleomycin lung injury model was established in Sprague-Dawley rats ($n = 12$). Human mesenchymal stem cells (hMSCs) labeled with QTracker655 were infused via jugular vein. After 2, 4, or 8 days, a second dose of hMSCs labeled with QTracker605 was infused, and animals were euthanized after 60, 120, or 240 minutes. Lungs, liver, spleen, heart, kidney, testis, and intestine were cryopreserved, followed by 3D cryo-imaging of each organ. At 60 minutes, 82% ± 9.7% of cells were detected; detection decreased to 60% ± 17% and 66% ± 22% at 120 and 240 minutes, respectively. At day 2, 0.06% of cells were detected, and this level remained constant at days 4 and 8 postinfusion. At 60, 120, and 240 minutes, 99.7% of detected cells were found in the liver, lungs, and spleen, with cells primarily retained in the liver. This is the first study using 3D cryo-imaging to track hMSCs in a rat lung injury model. hMSCs were retained primarily in the liver, with fewer detected in lungs and spleen. STEM CELLS TRANSLATIONAL MEDICINE *2016;5:1668–1675*

SIGNIFICANCE

Effective bench-to-bedside clinical translation of cellular therapies requires careful understanding of cell fate through tracking. Tracking cells is important to measure cell retention so that delivery methods and cell dose can be optimized and so that biodistribution and clearance can be defined to better understand potential off-target toxicity and redosing strategies. This article demonstrates, for the first time, the use of three-dimensional cryo-imaging for single-cell quantitative tracking of intravenous infused clinical-grade mesenchymal stem cells in a clinically relevant model of lung injury. The important information learned in this study will help guide future clinical and translational stem cell therapies for lung injuries.

INTRODUCTION

Effective bench-to-bedside clinical translation of cellular therapies requires careful understanding of cell fate through tracking. Tracking cells is important to measure (a) cell retention so that delivery methods/cell dose can be optimized and (b) biodistribution and clearance to define potential off-target toxicity and redosing strategies [1]. Unfortunately, cell tracking technology has been hampered by low sensitivity imaging incapable of detecting individual cells and lack of robust imaging labels to detect cells for longer than just the short term [2].

Several cell tracking methods have previously been described, each with certain pitfalls. Magnetic resonance imaging (MRI) can acutely visualize cells labeled with superparamagnetic iron oxide (SPION) or paramagnetic particles with a detection limit of approximately 1×10^4 cells [3–8]. The uptake of SPION by resident tissue macrophages tends to overestimate cell retention [9–11]. Positron emission tomography (PET) imaging can visualize radioactive markers such as [^{18}F]fluorodeoxyglucose

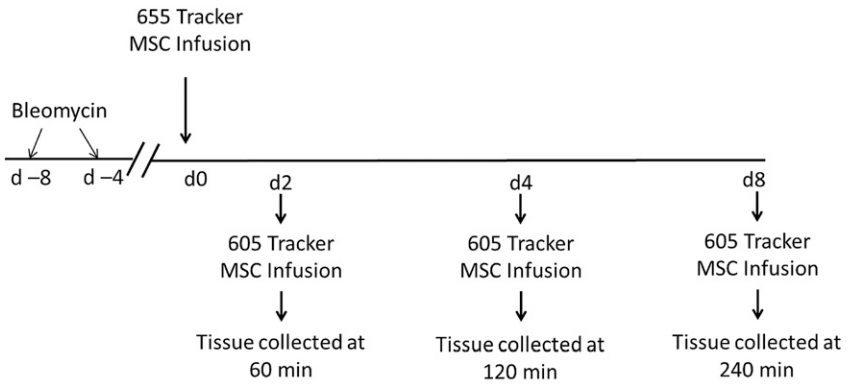

Cell Treatment Groups	# of Rats	655 Cell Infusion Time	605 Cell Infusion Time	Tissue Collected
Control (No Bleomyosin Treatment)	*n* = 3	Day 0	Day 2, 4, or 8	60,120, or 240 min on d2, d4, or d8
2 days post IV treatment	*n* = 3	Day 0	Day 2	60 min postinfusion on d2
4 days post IV treatment	*n* = 3	Day 0	Day 4	120 min postinfusion on d4
8 days post IV treatment	*n* = 3	Day 0	Day 8	240 min postinfusion on d8

Figure 1. Schematic of the study design. Animals were treated with bleomycin 4 days apart (days −8 and −4). On day 0, all animals received an intravenous infusion of human mesenchymal stem cells (hMSCs) loaded with QT655. On the day of assigned long-term tissue collection (day 2, 4, or 8) each animal received a second dose of hMSCs loaded with QT605. Animals were then euthanized at 60, 120, or 240 minutes after the infusion of QT605. Each group contains three animals for each time point except for the control animals, which had one animal at each time point. Abbreviations: d, day; MSC, mesenchymal stem cell.

(^{18}F-FDG) [12, 13]. Common radioactive labels such as ^{18}F-FDG have relatively short half-lives, limiting the tracking window to 10 hours postlabeling [14]. PET imaging has a detection limit of approximately 1×10^4 cells [15]. Single-photon emission computed tomography (SPECT) requires a radioactive label such as ^{111}indium oxine. ^{111}Indium oxine has a longer half-life than ^{18}F-FDG, allowing imaging for up to 4 days postlabeling [14]. However, SPECT is less sensitive than PET, with a limit of detection of approximately 1×10^5 cells [3]. Bioluminescence is an imaging method that detects light produced from a chemical reaction between an enzyme, such as luciferase, and its substrate, such as luciferin. To achieve this, cells are modified to express reporter genes such as *D-Luciferase*. Bioluminescence can be used to detect transplanted cells over time in vivo but is limited to studies in small animals because of high tissue absorption of emitted light [16]. Bioluminescence offers low-resolution two-dimensional images that must be coregistered to an anatomical reference image for context. The limit of cell detection with this method is approximately 1×10^3 cells [3].

Alternatively, fluorescence microscopy is an imaging method in which an emission light source of a specific wavelength causes dyes to fluoresce at different, yet predictable and detectable, wavelengths. Dyes such as quantum dots (Qdots, CellTracker) or reporter genes such as green fluorescence protein are introduced within the cells before transplantation. Although fluorescence microscopy is currently limited to ex vivo analyses, a major advantage is that it offers high-resolution imaging of single cells within intact tissues or whole animals. Furthermore, three-dimensional (3D) whole-organ fluorescence microscopy has been described [17–19].

Fluorescence microscopy using Qdots has been tested in a variety of cell types, including mesenchymal stem cells (MSCs) [20–22], embryonic stem cells [15, 23], pancreatic stem cells [24], and neural stem cells [25]. Qdots do not appear to adversely affect cell function and have minimal passive transfer to neighboring cells (<4%) in mixed culture or host tissues [21, 23, 26]. However, the detection window for Qdots varies greatly in the literature and is likely related to the cell type being tracked, the cell delivery method, and the disease model being studied.

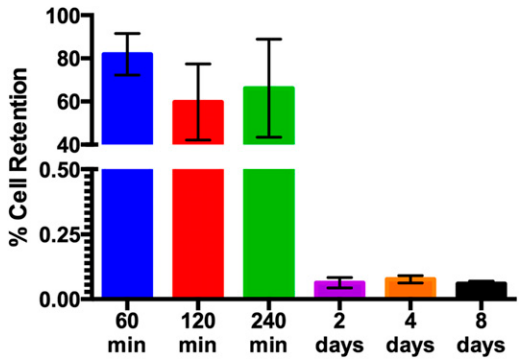

Figure 2. Overall human mesenchymal stem cell (hMSC) retention at short- and long-term time points. Short-term (60, 120, and 240 minutes after infusion) and long-term (2, 4, and 8 days after cell infusion) cell retention in all organs collected after an IV infusion of hMSCs. Data are presented as mean ± SEM of the percentage of cells detected in the tissue that was collected versus the total number of viable cells infused.

Our group is interested in testing the safety and therapeutic efficacy of intravenous infusion of MSCs to alleviate or slow the progression of bronchiolitis obliterans (BO) lung injury, which is a serious complication of lung transplantation. To this end, we have filed an investigational new drug (IND) application with the Food and Drug Administration (FDA) to test allogeneic MSC therapy to mitigate BO after lung transplantation. At the request of the FDA, we developed a preclinical model of BO [27]

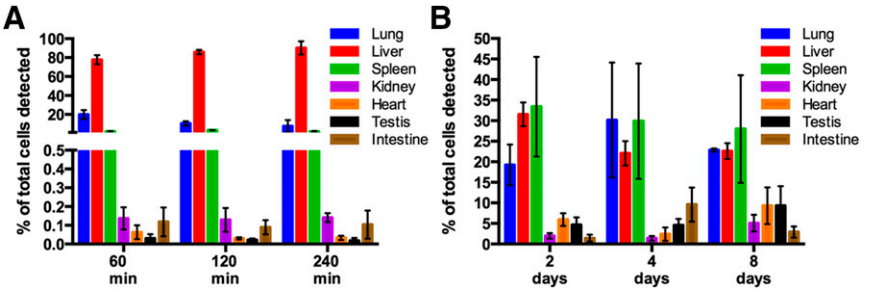

Figure 3. Biodistribution of human mesenchymal stem cells (hMSCs) at early and late time points. The total number of cells detected at each time point is represented as percentage of cells by location after an IV infusion of labeled hMSCs infused at 60, 120, and 240 minutes (early biodistribution) **(A)** and 2, 4, and 8 days (late biodistribution) **(B)**. Data are presented as mean ± SEM.

and a method to track MSCs and assess their biodistribution in this lung injury model. After discussion with the FDA panel and consideration of other models, bleomycin was determined to be the most representative and practical model to induce pathology similar to BO. Therefore, we exploited 3D fluorescence cryo-imaging microscopy with Qdot MSC labeling to measure retention and biodistribution in this relevant preclinical lung injury model.

Methods

Briefly, Qdot-labeled human MSCs (hMSCs) were infused intravenously in rats after the induction of a lung injury model previously described by our group [27]. Cell retention and biodistribution were measured over time. Details are described below.

MSC Production

The MSCs for these studies were produced by Waisman Biomanufacturing (Madison, WI, http://gmpbio.com) using a process that is comparable to that used for cGMP production of bone marrow (BM)-MSCs for human clinical trials [28]. A master cell bank was established at passage 2 using BM derived from a healthy donor. The BM harvest and consenting procedure were performed according to an institutional review board-approved protocol. Medical history was taken, and infectious disease testing was performed on the donor to comply with FDA Donor Eligibility requirements. MSCs were grown in media consisting of α-minimal essential medium with 10% fetal bovine serum and 1× Glutamax. Passaging was performed with TrypLE. The final MSC product was obtained by expanding MSCs from the passage 2 master cell bank to passage 5 in Cell Factories (Nunc). The final MSCs were tested for sterility (no contamination), endotoxins (<0.5 EU/ml), viability (>83% post-thaw), identity/purity (standard flow cytometry for MSC markers), and potency (immunopotency assay) as described [28]. MSCs were cryopreserved in a solution consisting of PlasmaLyte A (PL-A) with 2.5% dimethylsulfoxide and 10% human serum albumin and stored in the vapor phase of liquid nitrogen until used for these studies.

Rat Lung Injury Model

All animal procedures, including euthanasia methods, were approved by the institutional Animal Care and Use Committee. The double-dose bleomycin lung injury model was induced as recently described by our group [27]. Briefly, Sprague-Dawley Rats (n = 12) were anesthetized with 5% isoflurane and intubated, and an aerosol delivery device (MicroSprayer Aerosolizer; Penn Century, Wyndmoor, PA, http://penncentury.com) was inserted into the trachea. Normal sterile saline (200 μl) containing bleomycin (1.5 U/kg) was then delivered to both lungs. Animals received two doses of bleomycin administered 4 days apart (Fig. 1). Sham control animals (n = 3) received no aerosolized solution and were included at the request of the FDA.

Study Design

After induction of the lung injury model and 4 days after the second dose of bleomycin, rats were randomly assigned to receive two infusions of Qdot-labeled hMSCs. The first hMSC infusion was given on day 0 (4 days after the second bleomycin dose). These cells were labeled with QTracker 655 (QT655) to track cells at day 2, 4, or 8 (Fig. 1). The second hMSC infusion was given on day 2, 4, or 8. These cells were labeled with QTracker 605 (QT605) to track cells at 60, 120, and 240 minutes after infusion, and before the animals were euthanized and tissues were collected. Using the two different QTracker reporter wavelengths (655 and 605 nm), each rat was used to examine late, longer-term hMSC distribution (2, 4, or 8 days) and acute, early distribution (60, 120, or 240 minutes) (Fig. 1).

Cell Labeling Procedure

One-half milliliter of 6×10^6 hMSCs/ml was removed from liquid nitrogen storage and rapidly thawed in a 37°C water bath. hMSCs were washed twice by suspending in 5.5 ml PL-A and centrifuged at 1,000g for 10 minutes at 4°C. QTracker staining was carried out according to the manufacturer's instructions. Briefly, in a 1.5-ml tube, 3 μl reagent A was mixed with 3 μl reagent B (605 or 655), 600 μl PL-A was added, and the mixture was vortexed for 30 seconds. Immediately after the second washing, hMSCs were suspended in 300 μl PL-A, added to the CellTracker labeling solution, and incubated at 37°C for 55 minutes in the dark. After incubation, 600 μl PL-A was added to the cell suspension and centrifuged at 1,000g for 10 minutes at 4°C. The labeled hMSCs were then suspended in 1.5 ml PL-A and centrifuged at 1,000g for 10 minutes at 4°C. The Qdot-labeled hMSCs were split into two tubes each containing 1.2×10^6 cells and suspended in a volume of 1.3 ml PL-A. Cell viability was calculated before loading the cells for injection. A 25G needle was used to load the cells into a 3-ml syringe for infusion. hMSCs were held on ice in the dark until infused.

Cell Infusion Procedure

Rats were anesthetized with 5% isoflurane and maintained at 2% throughout the infusion procedure. An incision on the right anterior side of the neck was made, and the jugular vein was exposed. A butterfly catheter prefilled with the appropriate cell solution was inserted into the vein, and the MSC solution was infused

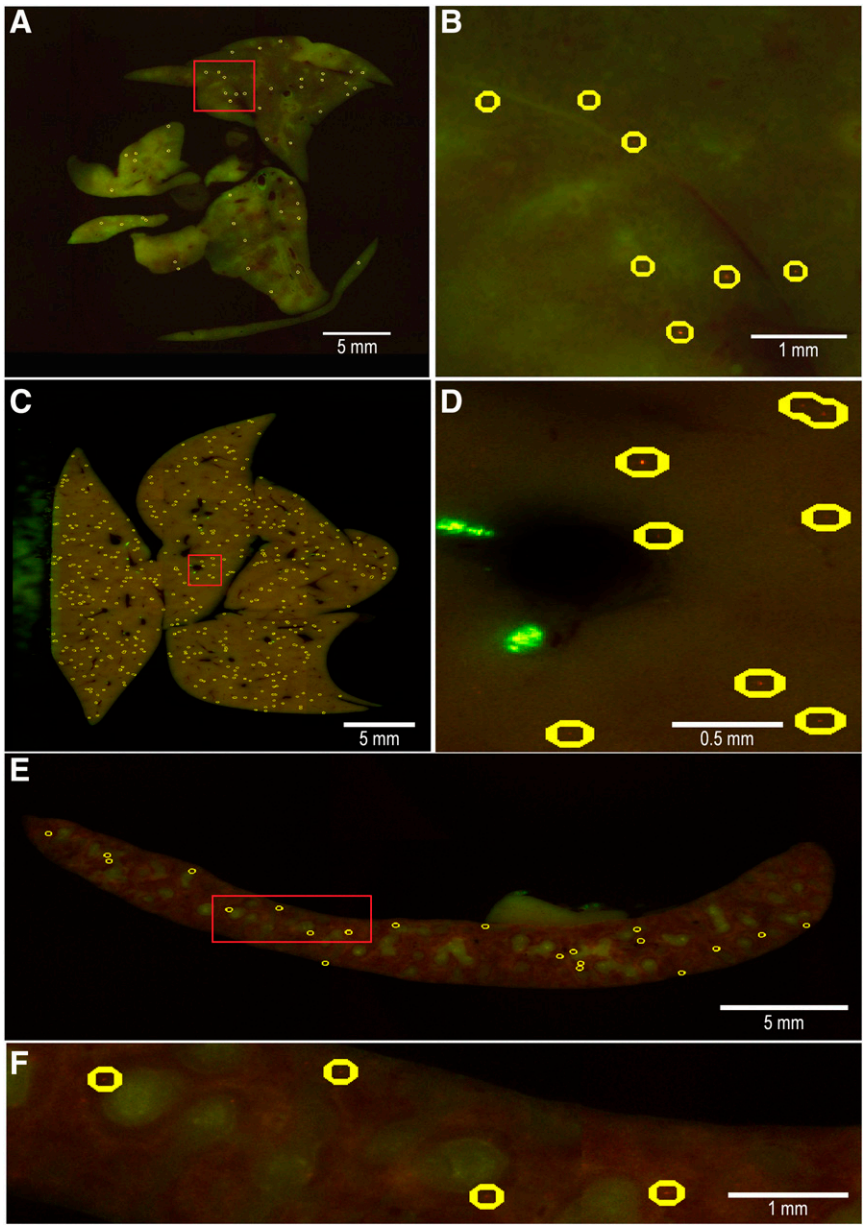

Figure 4. Representative fluorescence images with overlaid detected cells for different organs, along with zoomed-in views. **(A):** Lungs; yellow circles represent detected human mesenchymal stem cells (hMSCs). **(B):** Magnified image from red box in A. **(C):** Liver; yellow circles represent detected hMSCs. **(D):** Magnified image from red box in C. **(E):** Spleen; yellow circles represent detected hMSCs. **(F):** Magnified image from red box in E.

at a rate of 2.2 ml/hour (37 μl/minute). The syringe pump was inverted to prevent cells from settling against the syringe plunger. After infusion of 1.3 ml cell suspension, the infusion line was flushed with 0.5–0.7 ml saline, for a total infusion volume of 1.8–2 ml. Pressure was applied to the vein to stop bleeding, and the skin was closed. The left jugular vein was used for the second hMSC infusion according to the same procedure.

Necropsy and Whole-Organ Imaging

Upon sacrifice, the following organs were removed intact: lung, liver, spleen, kidney, heart, testis, and a portion of small intestine. The lungs, liver, spleen, heart, right kidney, right testis, and a section of the small intestine were frozen and stored (BioInVision, Cleveland, OH, http://www.bioinvision.com). Briefly, organs were placed in cryo-imaging embedding compound, frozen in liquid nitrogen vapor, and stored at −80°C until imaging. Whole-organ analysis was performed by serial sectioning and imaging of organs using the CryoViz cryo-imaging system (BioInVision). Section thickness was set to 40 μm, with an in-plane pixel size of 10.232 μm using an Olympus MVX-10 1× objective and ×0.63 magnification. Biodistribution of cells (CT605- and CT655-labeled hMSCs) was analyzed by coregistration of bright field and confocal images to generate a 3D whole-organ image reconstruction. Organs in which <200 cells were detected using automated detection were manually verified for accuracy.

A positive control was used to validate the dual-labeling technique and ensure spectral separation between first and second hMSC doses. To perform this validation, a healthy animal was euthanized, and the lungs were immediately excised. hMSCs (1×10^5) were

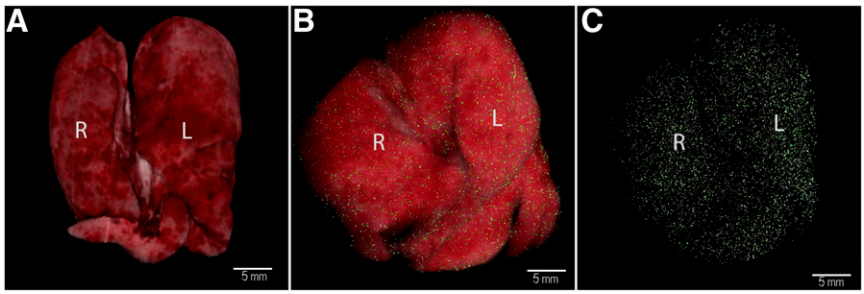

Figure 5. Intraorgan cellular biodistribution 60 minutes postinfusion. **(A):** 3D bright field reconstruction of lungs. **(B):** 3D bright field reconstruction with an overlay of detected mesenchymal stem cells (MSCs) from fluorescence. **(C):** 3D reconstruction showing detected MSCs from fluorescence.

labeled with QT605 or QT655, and a 50/50 mix (5.0×10^4 QT605 and 5.0×10^4 QT655) was directly injected into discrete lobes of the freshly excised lung. Immediately after injection into the lungs, the tissue was frozen and submitted for automated cell quantification. This tissue served as both positive and negative control, as cells were located in discrete areas, resulting in most sections being devoid of hMSCs (negative control).

Statistical Analysis

Data are presented as mean ± SEM. Student's *t* test was used to determine statistical differences between control animals and bleomycin-treated animals. *p* values less than .05 were considered statistically significant.

Results

Gross Necropsy

Animals treated with bleomycin had hemorrhagic areas throughout the lungs, but no other abnormalities were observed in other organs. Body weight and organ weights were not different between groups.

Cell Retention

Validation of Cell Retention in Excised Healthy Lung

Detection algorithms developed by BioInvision detected 88,607 of 100,000 QT605-labeled hMSCs, 72,000 of 100,000 QT655-labeled hMSCs, and 65,000 of 100,000 hMSCs in the QT605/QT655 lobe comprising 29,000 hMSC QT605-labeled and 36,000 QT655-labeled hMSCs. Because of suboptimal cutting, the lobes encompassing the QT655 and QT605/QT655 mix of hMSCs experienced debris on the surface of the tissue blocks. We estimated that 15% of cells were lost as a result of leakage of cells from the needle tract and within the dead space between the needle and syringe connection dead space.

Viability and In Vivo Cell Retention in Organs

Mean hMSC viability after thawing and QTracker labeling was 68% (±3%), resulting in an average infusion of 6.46×10^5 (±0.386) viable hMSCs at each time point. Mean total cell retention detected in organs at 60 minutes was 82.0% (±9.7%) and decreased to 60.0% (±17.6%) at 120 minutes and 66.0% (±22.7%) at 240 minutes (Fig. 2). By day 2 postinfusion, cell retention detected in organs fell to 0.06% of total viable hMSCs infused and remained constant until day 8.

Biodistribution

Early Biodistribution

At 60, 120, and 240 minutes postinfusion, 99.7% of the total cells detected were found in the liver, lungs, and spleen, with the remaining 0.3% of cells distributed in the kidney, heart, intestines, and testis (Figs. 3A, 4). Cell retention was consistently highest in the liver at 60, 120, and 240 minutes postinfusion, at 77.8% (±4.7%), 85.9% (±2.4%), and 90.2% (±7.0%), respectively. The lungs had the second highest cell retention rate at 60, 120, and 240 minutes, with 20.0% (±4.7%) 10.5% (±2.3%), and 7.6% (±6.5%) respectively. Finally, cell retention in the spleen was 2.0% (±0.4%), 3.3% (±0.1%), and 1.9% (±0.6%) at 60, 120, and 240 minutes postinfusion respectively. Intraorgan cellular biodistribution was uniform within the tissue (Fig. 5) (supplemental online Videos 1–3).

Late Biodistribution

The number of cells detected at 2, 4, and 8 days (*n* = 3 per time point) was less than 0.06% of the total cells infused on day 0. The mean number of cells detected in all tissues at day 2, 4, and 8 postinfusion was 361 (±120), 509 (±118) and 422 (±76), respectively. Of the cells detected on day 2, 19.2% ± 4.9% (60 ± 13 cells) were detected in the lungs, 31.5% ± 2.9% (112 ± 39 cells) in the liver, and 33.4% ± 12.1% (140 ± 63 cells) in the spleen. The remaining cells were variably distributed in the kidney (1.9% ± 0.7% [11 ± 1 cells]), heart (5.9% ± 1.5% [19 ± 6 cells]), intestines (1.4% ± 0.9% [6 ± 5 cells]), and testis (4.6% ± 1.8% [13 ± 2 cells]) (Figs. 3B, 6). Of the cells detected on day 4, 30.2% ± 14.0% (177 ± 108 cells) were detected in the lungs, 22.1% ± 3.0% (106 ± 17 cells) in the liver, and 29.9% ± 14.0% (141 ± 83 cells) in the spleen. The remaining cells were variably distributed in the kidney (1.4% ± 0.6% [6 ± 2 cells]), heart (2.4% ± 1.6% [14 ± 12 cells]), intestines (9.6% ± 4.2% [41 ± 10 cells]), and testis (4.5% ± 1.6% [24 ± 12 cells]). Of the cells detected on day 8, 22.8% ± 0.4% (97 ± 18 cells) were detected in the lungs, 22.6% ± 1.9% (93 ± 8 cells) in the liver, and 28.0% ± 13.1% (136 ± 82 cells) in the spleen. The remaining cells were variably distributed in the kidney (5.1% ± 2.1% [18 ± 6 cells]), heart (9.3% ± 4.4% [33 ± 15 cells]), intestines (2.9% ± 1.3% [12 ± 5 cells]), and testis (9.3% ± 4.7% [34 ± 15 cells]) (Fig. 6).

Early Lung Retention in Healthy and Diseased Lungs

We compared the retention of hMSCs in the lungs of healthy control rats at 60, 90, and 120 minutes to that of the bleomycin-treated rats at the same time points. Cell retention was numerically higher in the injured lungs (12.7% ± 2.0%, *n* = 9) compared with the healthy lungs (6.4% ± 3.0%, *n* = 3), although the difference was not statistically significant (*p* = .27) (Fig. 7).

Discussion

To our knowledge, this is the first study to use 3D whole-organ cryo-imaging to track intravenously infused hMSCs in an acute rat lung

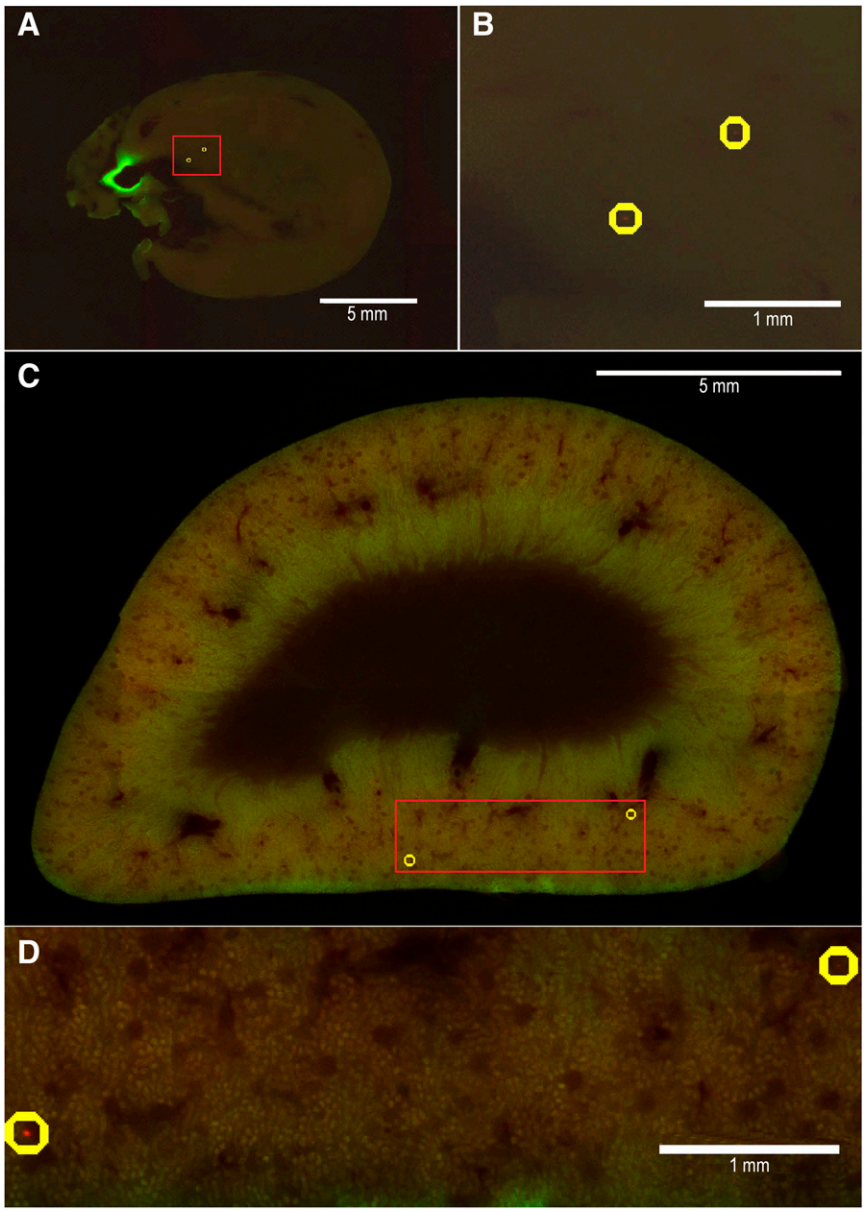

Figure 6. Representative fluorescence images with overlaid detected cells for different organs, along with zoomed-in views. **(A):** Heart; yellow circles represent detected human mesenchymal stem cells (hMSCs). **(B):** Magnified image from red box in A. **(C):** Kidney; yellow circles represent detected hMSCs. **(D):** Magnified image from red box in C.

injury model. A motivation behind this study was to measure cell biodistribution to support an FDA IND to permit clinical trials of MSCs for transplant-associated bronchiolitis obliterans. 3D whole-organ cryo-imaging is a sensitive method that provides accurate retention, biodistribution, and clearance information for infused hMSCs. Loading hMSCs with quantum dots of two distinct wavelengths (605 and 655 nm) allowed for acute and longer-term cell tracking within the same animal. Eighty percent of the infused labeled cells were detected within six organs at 1 hour post-infusion, falling to $<0.06\%$ by day 2 postinfusion. The ultrasensitive nature of 3D cryo-imaging allowed for single-cell detection in all organs tested (Figs. 4, 6). Organs were serially sectioned at 40 μm, significantly reducing sampling bias compared with other microscopy-based cell quantification techniques. Additionally, the Qdot wavelengths (605 and 655 nm) were specifically chosen to fall outside the range of typical tissue autofluorescence to reduce the likelihood of false discovery. Detection of 100% of the cell preparation is not expected, as cells are lost to priming of the delivery catheter, dead spaces in the syringe and fittings of the delivery system, as well as during placement of the catheter in the jugular vein. Additionally, because of sample size limitations, our cell tracking efforts were limited to a subset of selected organs. It is likely that a small percentage of infused MSCs are retained in the circulatory system and skeletal musculature and thus excluded from biodistribution and quantification analysis. For these reasons, biodistribution was calculated as a percentage of the total cells detected at each time point and not from the actual total number of cells delivered.

After intravenous infusion, hMSCs were primarily localized to the lungs, liver, and spleen, a finding that is similar to previous reports [29–32]. However, in our study, cell retention was highest in

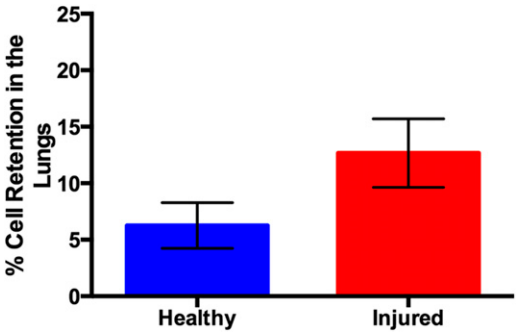

Figure 7. Percentage of cell retention at an early biodistribution (60, 120, and 240 minutes) in the lungs of healthy rats or those treated with two doses of bleomycin. Data presented as mean ± SEM (p = .27).

the liver, which is not consistent with previous reports that found higher acute cell retention in lungs [29, 30, 33–38]. For example, Fischer et al. found that nearly 99% of rat MSCs administered by intravenous infusion were initially retained in the lungs in a nondiseased rat model [29]. Similarly, in a mouse model of emphysema, Kim et al. showed that human adipose-derived MSCs were primarily retained in the lungs at 1 and 4 hours after intravenous infusion, which was further increased by the induction of emphysema [33]. This discrepant result may be caused by the differences in measurement time intervals, animal models, cell types, and cell-tracking methods. For example, studies using bioluminescence to track cells underestimate cell retention in the liver because of its high tissue absorption coefficient [39]. The increased liver tissue density results in greater light absorption compared with the lungs. Virostko et al. demonstrated that bioluminescence cell quantification is susceptible to changes/differences animal positioning, postsurgical effects, and light attenuation as a function of transplant site [40]. Changes in these variables may lead to an overestimation of cell retention in the lungs compared with the liver. Finally, PET and SPECT cell quantification is subject to multiple variables that may impact quantification accuracy, specifically, nonspecific uptake of radiolabels in the musculoskeletal system and artifacts related to inflammation, which may impact cell quantification accuracy [41, 42].

3D cryo-imaging offers single-cell sensitivity, which allows for accurate quantification and assessment of 3D biodistribution of infused cells. In contrast, PET, SPECT, MRI, or bioluminescence/fluorescence imaging modalities are considerably less sensitive than 3D cryo-imaging [3]. Interestingly, the presence of lung injury did not significantly boost cell retention in the lungs compared with healthy controls.

There are several limitations to this study. First, we used xenotransplantation of hMSCs into an immunocompetent rat lung injury model. Although several studies suggest that MSCs are immunoprivileged because of the relatively low expression of MHC class II and other and costimulatory proteins [43–47], there is the potential that an immune response could still be elicited. This is especially true when administering multiple MSCs doses, which could result in priming the immune system to target the second cell dose for clearance [48, 49]. We did not observe significant reductions in hMSCs between 60 and 240 minutes postinfusion, which would suggest that no significant immune system priming occurs in that short period of time. Second, the influence of quantum dot labeling on cell survival, proliferation, migration, or differentiation was not determined in this study. Previous Qdot labeling studies have not shown impaired survival, proliferation, migration or differentiation [15, 20–23]. Third, although Qdot dilution caused by cell division has not been shown to be a major component of the loss of Qdot signal over time [24, 50], we cannot rule out the potential loss of Qdot signal caused by MSC proliferation. Finally, we only tested MSCs and therefore, these findings may not be extended to other cell types.

Conclusion

3D cryo-imaging can be used to track single MSCs across a range of organs. Intravenous infusion of hMSCs in a rat lung injury model results in acute retention of cells primarily in the liver, lungs, and spleen, with few cells detected in the heart, kidney, intestine, or testis. hMSC retention is greatly reduced by 2 days postinfusion and remains relatively constant up to 8 days postinfusion. In our model, lung injury does not result in an increase in acute lung retention of infused hMSCs compared with normal uninjured lungs.

Acknowledgments

We thank Dr. Madhusudhana Gargesha and Dr. Debashish Roy of BioInvision Inc. for their thoughtful dialog regarding this project and careful review of the manuscript. This work was supported by the NIH/NHLBI Production Assistant for Cellular Therapies (PACT) contract number HHSN268201000010C.

Author Contributions

E.G.S. and J.M.K.: conception and design, collection and/or assembly of data, data analysis and interpretation, manuscript writing, final approval of manuscript; J.M.C. and A.N.R.: conception and design, data analysis and interpretation, manuscript writing, final approval of manuscript; T.A.H.: conception and design, collection and/or assembly of data, final approval of manuscript; R.K.B.: provision of study material or patients, collection and/or assembly of data, final approval of manuscript; M.E.: provision of study material or patients, final approval of manuscript; D.J.H.: conception and design, financial support, manuscript writing, final approval of manuscript; P.H.: conception and design, financial support, final approval of manuscript.

Disclosure of Potential Conflicts of Interest

The authors indicated no potential conflicts of interest.

References

1 Ankrum J, Karp JM. Mesenchymal stem cell therapy: Two steps forward, one step back. Trends Mol Med 2010;16:203–209.

2 Frangioni JV, Hajjar RJ. In vivo tracking of stem cells for clinical trials in cardiovascular disease. Circulation 2004;110:3378–3383.

3 Nguyen PK, Riegler J, Wu JC. Stem cell imaging: From bench to bedside. Cell Stem Cell 2014;14:431–444.

4 Neuwelt A, Sidhu N, Hu CA et al. Iron-based superparamagnetic nanoparticle contrast agents for MRI of infection and inflammation. AJR Am J Roentgenol 2015;204:W302–W313.

5 Mahmoudi M, Hosseinkhani H, Hosseinkhani M et al. Magnetic resonance imaging tracking of stem cells in vivo using iron oxide nanoparticles as a tool for the advancement of clinical regenerative medicine. Chem Rev 2011;111:253–280.

6 Li YQ, Tang Y, Fu R et al. Efficient labeling in vitro with non-ionic gadolinium magnetic resonance imaging contrast agent and fluorescent

transfection agent in bone marrow stromal cells of neonatal rats. Mol Med Rep 2015;12:913–920.

7 Tachibana Y, Enmi J, Agudelo CA et al. Long-term/bioinert labeling of rat mesenchymal stem cells with PVA-Gd conjugates and MRI monitoring of the labeled cell survival after intramuscular transplantation. Bioconjug Chem 2014;25:1243–1251.

8 Geng K, Yang ZX, Huang D et al. Tracking of mesenchymal stem cells labeled with gadolinium diethylenetriamine pentaacetic acid by 7T magnetic resonance imaging in a model of cerebral ischemia. Mol Med Rep 2015;11:954–960.

9 Huang Z, Li C, Yang S et al. Magnetic resonance hypointensive signal primarily originates from extracellular iron particles in the long-term tracking of mesenchymal stem cells transplanted in the infarcted myocardium. Int J Nanomedicine 2015;10:1679–1690.

10 Scharf A, Holmes S, Thoresen M et al. Superparamagnetic iron oxide nanoparticles as a means to track mesenchymal stem cells in a large animal model of tendon injury. Contrast Media Mol Imaging 2015;10:388–397.

11 Ma N, Cheng H, Lu M et al. Magnetic resonance imaging with superparamagnetic iron oxide fails to track the long-term fate of mesenchymal stem cells transplanted into heart. Sci Rep 2015;5:9058.

12 Blocklet D, Toungouz M, Berkenboom G et al. Myocardial homing of nonmobilized peripheral-blood CD34+ cells after intracoronary injection. STEM CELLS 2006;24:333–336.

13 Kang WJ, Kang HJ, Kim HS et al. Tissue distribution of 18F-FDG-labeled peripheral hematopoietic stem cells after intracoronary administration in patients with myocardial infarction. J Nucl Med 2006;47:1295–1301.

14 Wolfs E, Verfaillie CM, Van Laere K et al. Radiolabeling strategies for radionuclide imaging of stem cells. Stem Cell Rev 2015;11:254–274.

15 Lin S, Xie X, Patel MR et al. Quantum dot imaging for embryonic stem cells. BMC Biotechnol 2007;7:67.

16 de Almeida PE, van Rappard JR, Wu JC. In vivo bioluminescence for tracking cell fate and function. Am J Physiol Heart Circ Physiol 2011; 301:H663–H671.

17 Steyer GJ, Roy D, Salvado O et al. Cryo-imaging of fluorescently-labeled single cells in a mouse. Proc SPIE Int Soc Opt Eng 2009;7262: 72620W–72620W-8. doi:10.1117/12.812982

18 Steyer GJ, Roy D, Salvado O et al. Removal of out-of-plane fluorescence for single cell visualization and quantification in cryo-imaging. Ann Biomed Eng 2009;37:1613–1628.

19 Bentolila LA, Ebenstein Y, Weiss S. Quantum dots for in vivo small-animal imaging. J Nucl Med 2009;50:493–496.

20 Ohyabu Y, Kaul Z, Yoshioka T et al. Stable and nondisruptive in vitro/in vivo labeling of mesenchymal stem cells by internalizing quantum dots. Hum Gene Ther 2009;20:217–224.

21 Rosen AB, Kelly DJ, Schuldt AJ et al. Finding fluorescent needles in the cardiac haystack: Tracking human mesenchymal stem cells labeled with quantum dots for quantitative in vivo three-dimensional fluorescence analysis. STEM CELLS 2007;25:2128–2138.

22 Seleverstov O, Zabirnyk O, Zscharnack M et al. Quantum dots for human mesenchymal stem cells labeling. A size-dependent autophagy activation. Nano Lett 2006;6:2826–2832.

23 Rak-Raszewska A, Marcello M, Kenny S et al. Quantum dots do not affect the behaviour of mouse embryonic stem cells and kidney stem cells and are suitable for short-term tracking. PLoS One 2012;7:e32650.

24 Danner S, Benzin H, Vollbrandt T et al. Quantum dots do not alter the differentiation potential of pancreatic stem cells and are distributed randomly among daughter cells. Int J Cell Biol 2013;2013:918242.

25 Slotkin JR, Chakrabarti L, Dai HN et al. In vivo quantum dot labeling of mammalian stem and progenitor cells. Dev Dyn 2007;236:3393–3401.

26 Niu X, Gupta K, Yang JT et al. Physical transfer of membrane and cytoplasmic components as a general mechanism of cell-cell communication. J Cell Sci 2009;122:600–610.

27 Braun RK, Koch JM, Hacker TA et al. Cardiopulmonary and histological characterization of an acute rat lung injury model demonstrating safety of mesenchymal stromal cell infusion. Cytotherapy 2016;18:536–545.

28 Bloom DD, Centanni JM, Bhatia N et al. A reproducible immunopotency assay to measure mesenchymal stromal cell-mediated T-cell suppression. Cytotherapy 2015;17:140–151.

29 Fischer UM, Harting MT, Jimenez F et al. Pulmonary passage is a major obstacle for intravenous stem cell delivery: The pulmonary first-pass effect. Stem Cells Dev 2009;18:683–692.

30 Barbash IM, Chouraqui P, Baron J et al. Systemic delivery of bone marrow-derived mesenchymal stem cells to the infarcted myocardium: Feasibility, cell migration, and body distribution. Circulation 2003;108:863–868.

31 Chin BB, Nakamoto Y, Bulte JW et al. 111In oxine labelled mesenchymal stem cell SPECT after intravenous administration in myocardial infarction. Nucl Med Commun 2003;24: 1149–1154.

32 Detante O, Moisan A, Dimastromatteo J et al. Intravenous administration of 99mTc-HMPAO-labeled human mesenchymal stem cells after stroke: In vivo imaging and biodistribution. Cell Transplant 2009;18:1369–1379.

33 Kim YS, Kim JY, Shin DM et al. Tracking intravenous adipose-derived mesenchymal stem cells in a model of elastase-induced emphysema. Tuberc Respir Dis (Seoul) 2014;77:116–123.

34 Gao J, Dennis JE, Muzic RF et al. The dynamic in vivo distribution of bone marrow-derived mesenchymal stem cells after infusion. Cells Tissues Organs 2001;169:12–20.

35 Allers C, Sierralta WD, Neubauer S et al. Dynamic of distribution of human bone marrow-derived mesenchymal stem cells after transplantation into adult unconditioned mice. Transplantation 2004;78:503–508.

36 Tolar J, O'shaughnessy MJ, Panoskaltsis-Mortari A et al. Host factors that impact the biodistribution and persistence of multipotent adult progenitor cells. Blood 2006;107:4182–4188.

37 Meyerrose TE, De Ugarte DA, Hofling AA et al. In vivo distribution of human adipose-derived mesenchymal stem cells in novel xenotransplantation models. STEM CELLS 2007;25:220–227.

38 Schrepfer S, Deuse T, Reichenspurner H et al. Stem cell transplantation: The lung barrier. Transplant Proc 2007;39:573–576.

39 Cheong WF, Prahl SA, Welch AJ. A review of the optical properties of biological tissues. IEEE J Quantum Electron 1990;26:2166–2185.

40 Virostko J, Chen Z, Fowler M et al. Factors influencing quantification of in vivo bioluminescence imaging: Application to assessment of pancreatic islet transplants. Mol Imaging 2004;3: 333–342.

41 Cook GJ, Fogelman I, Maisey MN. Normal physiological and benign pathological variants of 18-fluoro-2-deoxyglucose positron-emission tomography scanning: potential for error in interpretation. Semin Nucl Med 1996;26:308–314.

42 Cook GJ, Wegner EA, Fogelman I. Pitfalls and artifacts in 18FDG PET and PET/CT oncologic imaging. Semin Nucl Med 2004;34:122–133.

43 Ryan JM, Barry FP, Murphy JM et al. Mesenchymal stem cells avoid allogeneic rejection. J Inflamm (Lond) 2005;2:8.

44 Zimmet JM, Hare JM. Emerging role for bone marrow derived mesenchymal stem cells in myocardial regenerative therapy. Basic Res Cardiol 2005;100:471–481.

45 Atoui R, Shum-Tim D, Chiu RC. Myocardial regenerative therapy: Immunologic basis for the potential "universal donor cells". Ann Thorac Surg 2008;86:327–334.

46 Pittenger MF, Martin BJ. Mesenchymal stem cells and their potential as cardiac therapeutics. Circ Res 2004;95:9–20.

47 Dai W, Hale SL, Martin BJ et al. Allogeneic mesenchymal stem cell transplantation in post-infarcted rat myocardium: short- and long-term effects. Circulation 2005;112:214–223.

48 Ankrum JA, Ong JF, Karp JM. Mesenchymal stem cells: Immune evasive, not immune privileged. Nat Biotechnol 2014;32:252–260.

49 Schmuck EG, Koch JM, Hacker TA et al. Intravenous followed by X-ray fused with MRI-guided transendocardial mesenchymal stem cell injection improves contractility reserve in a swine model of myocardial infarction. J Cardiovasc Transl Res 2015;8:438–448.

50 Pi QM, Zhang WJ, Zhou GD et al. Degradation or excretion of quantum dots in mouse embryonic stem cells. BMC Biotechnol 2010; 10:36.

See www.StemCellsTM.com for supporting information available online.

